The 2009 IEEE/RSJ International Conference on
Intelligent Robots and Systems
October 11-15, 2009 St. Louis, USA

Biped Walking Control Based on Hybrid Position/Force Control

Thomas Buschmann, Sebastian Lohmeier and Heinz Ulbrich

***Abstract*— This paper describes a real-time walking control system developed for the biped robots *JOHNNIE* and *LOLA*. Walking trajectories are planned on-line using a simplified robot model and modified by a stabilizing controller. The controller uses hybrid position/force control in task space based on a resolved motion rate scheme. Inertial stabilization is achieved by modifying the contact force trajectories. The paper includes an analysis of the dynamics of controlled bipeds, which is the basis for the proposed control system. The system was tested both in forward dynamics simulations and in experiments with *JOHNNIE*.**

I. Introduction

Both the commercial potential of humanoid robots in the service and entertainment industries [1] and interesting research topics in hardware design and control have lead to the development of a number of sophisticated humanoid robots by companies [2], [3] and academic institutions [4]–[7]. For many potential applications reliable, fast and flexible biped locomotion is a basic requirement.

In this paper we describe a walking control system developed for the biped robots *JOHNNIE* (Fig. 8) and *LOLA* (Fig. 1). We give an overview of related work in biped walking control and the control of robot manipulators (Section II). Based on an analysis of the control problem (Section III) we describe the basic control strategy and give a derivation of the proposed control law (Section IV). Finally, we show results from dynamics simulations of *LOLA* and walking experiments with *JOHNNIE* (Section V).

II. Related Work

A. Control of Biped Locomotion

The most common method of biped walking control is to first calculate theoretically stable walking patterns either on-line [8], [9] or off-line [10]. The trajectory is then modified on-line using feedback control in order to achieve stable walking.

A large number of methods for stabilizing control of bipeds have been proposed and a number of similar ideas have been successfully implemented on full-size humanoid robots. Without attempting to review all methods, we briefly describe the ones we consider to be the most relevant to our approach.

A common strategy for stabilizing the upper body inclination is to control the contact torques at the feet [6], [11], [12]. Usually, the foot torques are measured by six-axis force/torque sensors and controlled via position control of the ankle joints. Another common strategy is to accelerate the center of mass (CoM), creating a reaction force that stabilizes the robot [3], [13].

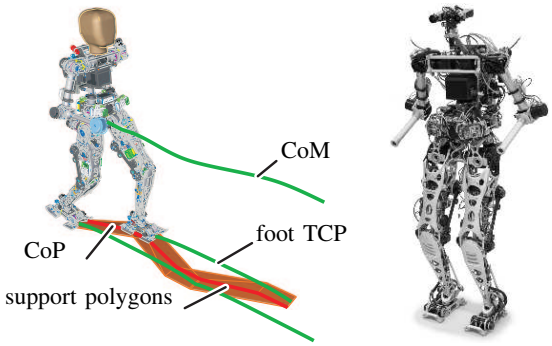

Fig. 1. Snapshot of simulation of *LOLA* walking with the proposed control system with trajectory planning results overlaid (left) and photograph of *LOLA* (right).

An interesting strategy for stabilizing planar bipeds based on methods for torque limited control of robot manipulators [14] was proposed in [15]. By using time scaling of the trajectory, both the geometric path and the center of pressure (CoP) can be tracked. However, since time scaling only adds one additional control input, application to three dimensional robots is not straightforward.

In order to reduce landing impacts, many robots also incorporate an active control of vertical contact forces. This can be achieved by measuring the contact force and changing position set points [6], [11]. Another strategy involves reducing joint position control gains during initial contact [3], [16], i.e. using indirect force control.

Fujimoto proposed a hybrid position/force control scheme based on task space position control [17]. Contact torques in the ground plane are used for tracking a reference CoP and not for stabilizing the robot. The remaining contact forces are used for controlling the robot's pose and torso height. Contrary to our approach, stabilization of the CoM trajectory is achieved by modifying the swing leg trajectory according to Kajita's *Linear Inverted Pendulum Mode* [18].

Löffler proposed an approach based on feedback linearization for the biped *JOHNNIE*. The performance of this method was limited by the available sensor bandwidth, computational power and accuracy of the models, so the performance of a method based on Impedance Control proved to be superior [6].

This work is supported by the "Deutsche Forschungsgemeinschaft" (grant UL105/29).

The authors are with the *Institute of Applied Mechanics, Technische Universität München,* Bolzmannstr. 15, Garching, Germany. E-mail: {buschmann, lohmeier, ulbrich}@amm.mw.tum.de

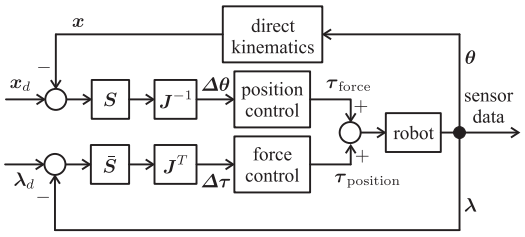

Fig. 2. Hybrid position/force control for a torque controlled device, as proposed in [19]. $\boldsymbol{S}, \bar{\boldsymbol{S}}$ denote the selection matrices for position and force controlled dimensions respectively.

B. Hybrid Position/Force Control

Hybrid position/force control was originally proposed by CRAIG and RAIBERT for interaction control of robot manipulators [19]. The basic approach is to partition the task space into force and position controlled sub-spaces according to the geometry of the assembly or manipulation problem. This allows precise motion control in unconstrained directions while force control leads to an adaptation of the robot's motion to the environment's geometry and stiffness.

In [19] the individual joint control terms are a linear combination of contributions from a PID-type position control and direct force control (cf. Fig. 2). More sophisticated approaches using dynamics models of the manipulator and nonlinear decoupling were subsequently proposed by KHATIB [20] and others.

Classically, hybrid position/force control was formulated for torque controlled manipulators. However, for robots with high structural stiffness, actuated by electric motors through reduction gears with relatively high ratios (≥ 50), decoupled joint position control often leads to more than adequate motion control performance. Furthermore, direct joint position control enables good disturbance rejection and compensation of gear friction with high bandwidth [21]. This has led to the development of hybrid position/force control based on inner position or velocity control loops [22, Ch. 7].

III. PROBLEM ANALYSIS AND SYSTEM OVERVIEW

In this section we present a simplified dynamics model of our robot and use it to identify two basic challenges in biped walking control: determining physically feasible motions and dealing with the underactuation of the robot. Based on this analysis, we describe the basic structure of our walking control system.

A. Problem Analysis

To analyze the walking control problem, we model the robot as a rigid multibody system (MBS) with compliant, unilateral ground contact:

$$\boldsymbol{M}\ddot{\boldsymbol{q}} + \boldsymbol{h} = \boldsymbol{W}_\tau \boldsymbol{\tau} + \boldsymbol{W}_\lambda \boldsymbol{\lambda} \tag{1}$$

$$\boldsymbol{C}_i \boldsymbol{d}_i = \boldsymbol{f}_i \quad \forall i \in I_c \tag{2}$$

$$\boldsymbol{g}_{\text{IE}}(\boldsymbol{f}, \boldsymbol{q}) \geq 0 \tag{3}$$

$$\boldsymbol{\lambda} = \sum_i \boldsymbol{T}_{f,i} \boldsymbol{f}_i \tag{4}$$

Here $\boldsymbol{M}$ and $\boldsymbol{h}$ are the mass matrix and the vector of smooth forces respectively and $\boldsymbol{q}$ are the generalized coordinates. $\boldsymbol{W}_\tau$ and $\boldsymbol{W}_\lambda$ are the Jacobians of the contact forces $\boldsymbol{\lambda}$ and joint torques $\boldsymbol{\tau}$. The contact with the environment is modeled as a set of point contacts with forces $\boldsymbol{f}_i$, deformations $\boldsymbol{d}_i$ and stiffness $\boldsymbol{C}_i$. The resulting contact force vector $\boldsymbol{\lambda} \in \mathbb{R}^{12}$ that can be measured by the two six-axis force/torque sensors, is calculated from the individual contact forces $\boldsymbol{f}_i$ using the transform matrix $\boldsymbol{T}_{f,i} \in \mathbb{R}^{6\times 3}$, which depends on the position of $\boldsymbol{f}_i$ relative to the force sensor reference frame.

Conditions from the unilateral contact are summed up in the vector inequality $\boldsymbol{g}_{\text{IE}}$. $\boldsymbol{\lambda}$ is determined by summing over all i in the set of active contacts I_c.

Due to the unilateral ground contact (3) not all robot motions are feasible. This is one of the basic difficulties in biped walking control. One solution is to generate physically feasible walking patterns on-line using an adequate motion planning algorithm. Our implementation of this strategy is described in [8].

Theoretically, perfect tracking of planned trajectories leads to stable walking. However, disturbances and modeling errors of both robot and environment inevitably lead to deviations from the ideal walking trajectory.

Due to the compliant ground contact, the joint torque Jacobian does not have full rank:

$$\boldsymbol{W}_\tau = \begin{bmatrix} \boldsymbol{0}^{6\times n} \\ \boldsymbol{W}_{\tau,2} \end{bmatrix} \tag{5}$$

That is, the first six degrees of freedom (DoFs) $\boldsymbol{q}_1$ corresponding to the robot's upper body position and orientation cannot be directly controlled, i.e. the system is underactuated. From (1) it is apparent that we can control $\boldsymbol{q}_1$ either via $\boldsymbol{\lambda}$ or $\boldsymbol{h}$. Since accelerating the CoM is equivalent to changing the horizontal contact force, both this strategy and ankle torque control rely on manipulating $\boldsymbol{\lambda}$ for stabilizing the robot.

B. System Overview

The basic structure of the real-time walking control system is shown in Fig. 3. General control commands are input via a finite state machine (FSM) that coordinates the entire walking control system. Depending on the FSM's state, planning and control modules are selected and configured.

Based on a desired walking direction and speed, a sequence of three walking steps is planned. The step sequence is represented as an array of walking parameters that serve as input to the walking pattern generator. The step sequence planner uses tables generated off-line to choose parameter combinations of step length, step frequency, double support period etc. leading to smooth and stable walking [8].

The step sequence is used for generating walking trajectories $\boldsymbol{x}_{id}$ in task space. Table I summarizes the definition of $\boldsymbol{x}_{id}$ for *LOLA*. For both *LOLA* and *JOHNNIE* we control the CoM trajectory according to the MBS model, not the torso position.

Using data from the inertial measurement unit (IMU), the force torque sensors and the current state of the robot, the desired contact forces $\boldsymbol{\lambda}$ are modified (cf. Section IV-A).

TABLE I

TRAJECTORY PARAMETRIZATION FOR *LOLA*

right foot from robot CoM	$\boldsymbol{r}_{\mathrm{LR}} - \boldsymbol{r}_{\mathrm{CoM}}$
left foot from robot CoM	$\boldsymbol{r}_{\mathrm{LL}} - \boldsymbol{r}_{\mathrm{CoM}}$
relative right foot/upper body orientation	$\boldsymbol{\varphi}_{\mathrm{LR}}$
relative left foot/upper body orientation	$\boldsymbol{\varphi}_{\mathrm{LL}}$
right arm CoM from robot CoM	$\boldsymbol{r}_{\mathrm{AR}} - \boldsymbol{r}_{\mathrm{CoM}}$
left arm CoM from robot CoM	$\boldsymbol{r}_{\mathrm{AL}} - \boldsymbol{r}_{\mathrm{CoM}}$
upper body orientation	$\boldsymbol{\varphi}_{\mathrm{UB}}$
robot CoM from stance foot	$\boldsymbol{r}_{\mathrm{CoM}}$

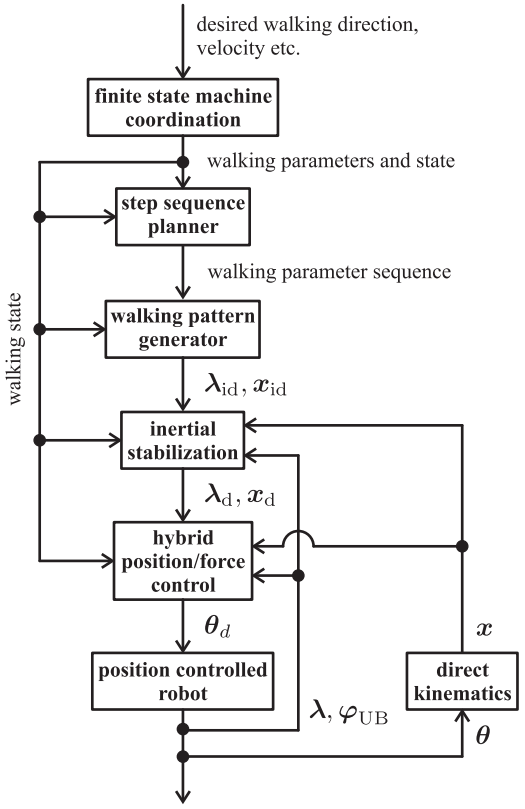

Fig. 3. Structure of the real-time walking control system.

Desired contact forces and remaining task space dimensions are controlled using a hybrid force position control scheme based on an inner position control loop (cf. Section IV-B).

IV. STABILIZING CONTROL

For stabilizing control, we propose a generalization of the Impedance Control method previously used for *JOHNNIE* [6]. Based on the analysis in Section III, we modify the desired contact forces $\boldsymbol{\lambda}_{id}$ in order to stabilize $\boldsymbol{q}_1$.

The theoretical justification for this approach derives from the fact that (1) has pronounced slow-fast dynamics. If we assume for simplicity that the contact state does not change and partition the degrees of freedom into six upper body DoFs $\boldsymbol{q}_1$ and $n-6$ joint angles $\boldsymbol{q}_2 = \boldsymbol{\theta}$, the system can be rewritten as:

$$\boldsymbol{M}_{11}\ddot{\boldsymbol{q}}_1 + \boldsymbol{M}_{12}\ddot{\boldsymbol{q}}_2 + \tilde{\boldsymbol{h}}_1 = \boldsymbol{0} \tag{6}$$

$$\boldsymbol{M}_{21}\ddot{\boldsymbol{q}}_1 + \boldsymbol{M}_{22}\ddot{\boldsymbol{q}}_2 + \tilde{\boldsymbol{h}}_2 = \boldsymbol{0} \tag{7}$$

Here $\tilde{\boldsymbol{h}}_1, \tilde{\boldsymbol{h}}_2$ include contact forces and joint torques. The structure of the dynamics of the controlled robot becomes more apparent by scaling the EoM so the norm of the force vectors $\|\tilde{\boldsymbol{h}}_i\|$ are in the order of 1:

$$\frac{1}{\sigma_{\boldsymbol{M}_{11}}\sigma_{\boldsymbol{h}_1}}\boldsymbol{M}_{11}\ddot{\boldsymbol{q}}_1 + \frac{1}{\sigma_{\boldsymbol{M}_{11}}\sigma_{\boldsymbol{h}_1}}(\boldsymbol{M}_{12}\ddot{\boldsymbol{q}}_2 + \tilde{\boldsymbol{h}}_1) = \boldsymbol{0} \tag{8}$$

$$\frac{1}{\sigma_{\boldsymbol{M}_{11}}\sigma_{\boldsymbol{h}_2}}\boldsymbol{M}_{22}\ddot{\boldsymbol{q}}_2 + \frac{1}{\sigma_{\boldsymbol{M}_{11}}\sigma_{\boldsymbol{h}_2}}(\boldsymbol{M}_{21}\ddot{\boldsymbol{q}}_2 + \tilde{\boldsymbol{h}}_2) = \boldsymbol{0}. \tag{9}$$

Here $\sigma_{\boldsymbol{M}_{11}} \approx \|\boldsymbol{M}_{11}\|$ and $\sigma_{\boldsymbol{h}_i} \approx \|\partial \boldsymbol{h}_i/\partial \boldsymbol{q}\|$. The structure of the MBS leads to $\|\boldsymbol{M}_{11}\| / \|\boldsymbol{M}_{22}\| \gg 1$ and $\|\boldsymbol{M}_{12}\| / \|\boldsymbol{M}_{11}\| \gg 1$, while the inequality $\|\sigma_{\boldsymbol{h}_2}\| \gg 1$ is even more pronounced due to the high gain joint position control. In sum $\|\frac{1}{\sigma_{\boldsymbol{M}_{11}}\sigma_{\boldsymbol{h}_2}}\boldsymbol{M}_{22}\| \ll 1$ while $\|\frac{1}{\sigma_{\boldsymbol{M}_{11}}\sigma_{\boldsymbol{h}_1}}\boldsymbol{M}_{11}\| \approx 1$. We denote the nominal walking trajectory by $\boldsymbol{q}_{1,id}, \boldsymbol{q}_{2,id}$. Then, in the terminology of singular perturbation theory, we can describe $\boldsymbol{q}_1 - \boldsymbol{q}_{1,id}$ as the slow manifold, while $\boldsymbol{q}_2 - \boldsymbol{q}_{2,id}$ is the fast manifold.

Based on the preceding analysis, we divide the robot's control into a slow and a fast component. We start by partitioning $\boldsymbol{x}$ into $\boldsymbol{x}_{\mathrm{IN}}^T = (\boldsymbol{\varphi}_{\mathrm{UB}}^T, \boldsymbol{r}_{\mathrm{CoM}}^T)$ and $\boldsymbol{x}_{\mathrm{REL}}$, where $\boldsymbol{x}_{\mathrm{IN}}$ depends on both $\boldsymbol{q}_1$ and $\boldsymbol{q}_2$ and $\boldsymbol{x}_{\mathrm{REL}}$ depends only on $\boldsymbol{q}_2$. In the slow module we then stabilize $\boldsymbol{x}_{\mathrm{IN}}$ via $\boldsymbol{\lambda}$, while the fast module controls $\boldsymbol{x}_{\mathrm{REL}}$ and $\boldsymbol{\lambda}$ via $\boldsymbol{q}_2$.

A. Contact Force Modification

For stabilizing $\boldsymbol{x}_{\mathrm{IN}}$ we adopt a simple PD-type control with saturation:

$$\boldsymbol{\lambda}_d = \mathrm{sat}\,(\boldsymbol{\lambda}_{id} + \boldsymbol{K}_P \boldsymbol{\Delta}\boldsymbol{x}_{\mathrm{IN}} + \boldsymbol{K}_D \boldsymbol{\Delta}\dot{\boldsymbol{x}}_{\mathrm{IN}}). \tag{10}$$

sat is the saturation function used to obtain only physically feasible contact force references $\boldsymbol{\lambda}_d$. Boundaries of admissible force setpoints are calculated from the foot geometry, the current force sensor signal and the current state of the walking FSM.

The control gains $\boldsymbol{K}_P, \boldsymbol{K}_D$ are calculated by the walking pattern generator and are responsible for distributing the overall contact force between left and right foot during double support.

B. Hybrid Position/Force Control

For real-time control, the foot-ground contact is modeled as a set of decoupled point contacts with stiffness $\boldsymbol{C}_i$ and negligible damping (cf. Fig. 4). By using an explicit contact model, changing foot geometries, contact states and contact stiffness can easily be taken into account, which is usefull for *LOLA* during heel or toe contact. A further advantage is the fact that the terms in the force control equations have a clear physical meaning. More importantly, control of individual force components is decoupled. If the foot's "tool center point" and/or the force sensor is not at the center of the foot or the foot's contact stiffness is not homogeneous, controlling only the rotation of the foot relative to the upper body or only the ankle joints will generally alter both the contact torque and the normal contact force. This is avoided by taking the foot geometry, contact stiffness and force sensor location into account.

Using the known contact state, i. e. which contacts are opened or closed, the total force $\boldsymbol{F}_j$ and torque $\boldsymbol{T}_j$ acting on foot j are given by

$$\begin{pmatrix} \boldsymbol{F}_j \\ \boldsymbol{T}_j \end{pmatrix} = \sum_{i \in I_{c,j}} \begin{pmatrix} {}_j\boldsymbol{C}_i \, \boldsymbol{d}_{c,i} \\ {}_j\boldsymbol{\Delta r}_{c,i} \times {}_j\boldsymbol{C}_i \, \boldsymbol{d}_{c,i} \end{pmatrix} \tag{11}$$

where $I_{c,j}$ denotes the subset of I_c on foot j, $\boldsymbol{d}_{c,i}$ is the deformation of the i-th contact element and ${}_j\boldsymbol{\Delta r}_{c,i}$ is the vector from the force sensor frame to the contact element.

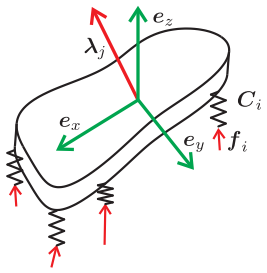

Fig. 4. Contact model for stabilizing control.

Similar to the use of a binary selection vector by CRAIG *et al.* to specify force or position controlled dimensions [19], we use selection matrices to specify subsets of $\boldsymbol{\lambda}$ and $\boldsymbol{x}$ to be actively controlled:

$$\boldsymbol{\lambda}_c = \boldsymbol{S}_\lambda \boldsymbol{\lambda} \tag{12}$$

$$\boldsymbol{x}_c = \boldsymbol{S}_x \boldsymbol{x} \tag{13}$$

Here the subscript c denotes the actively controlled variables and $\boldsymbol{S}_\lambda, \boldsymbol{S}_x$ are binary selection matrices. Currently, we actively control the forces normal to and the torques in the contact plane.

In the non-position controlled dimensions we allow a modification of the reference trajectories by $\boldsymbol{\Delta \dot{x}}_\lambda$ for force control. With $\boldsymbol{K}_\lambda$ as a control gain, we choose the linear error dynamics

$$\boldsymbol{S}_\lambda \left(\boldsymbol{\Delta \dot{\lambda}} + \boldsymbol{K}_\lambda \boldsymbol{\Delta \lambda} \right) = 0 \tag{14}$$

for the actively controlled forces. With $\bar{\boldsymbol{S}}_x$ denoting the complement of $\boldsymbol{S}_x$, we have

$$\boldsymbol{\Delta \dot{x}}_\lambda = \bar{\boldsymbol{S}}_x \boldsymbol{\nabla}_q \boldsymbol{x} \dot{\boldsymbol{q}}_{\boldsymbol{\Delta \dot{x}}_\lambda}. \tag{15}$$

From the contact model (11) we obtain the relationship:

$$\boldsymbol{\dot{\lambda}} = \boldsymbol{\nabla}_q \boldsymbol{\lambda} \dot{\boldsymbol{q}} \tag{16}$$

Substituting (16) into (14) and rearranging yields:

$$\left(\boldsymbol{S}_\lambda \boldsymbol{\nabla}_q \boldsymbol{\lambda} \right) \dot{\boldsymbol{q}} = \boldsymbol{S}_\lambda \left(\boldsymbol{\lambda}_d + \boldsymbol{K}_\lambda \boldsymbol{\Delta \lambda} \right) \tag{17}$$

Because of the linear relationship between generalized velocities and workspace velocities we have $\dot{\boldsymbol{q}} = \dot{\boldsymbol{q}}_{id} + \dot{\boldsymbol{q}}_{\Delta \dot{\boldsymbol{x}}_\lambda}$, where $\dot{\boldsymbol{q}}_{id}$ are the ideal generalized velocities corresponding to $\dot{\boldsymbol{x}}_{id}$. Using this relationship and the MOORE-PENROSE pseudoinverse $(\cdot)^\dagger$ we can solve for the trajectory modification:

$$\begin{aligned} \boldsymbol{\Delta \dot{x}}_\lambda = &\left(\boldsymbol{S}_\lambda \boldsymbol{\nabla}_q \boldsymbol{\lambda} \left(\bar{\boldsymbol{S}}_x \boldsymbol{\nabla}_q \boldsymbol{x} \right)^\dagger \right)^\dagger \\ &\boldsymbol{S}_\lambda \left(\boldsymbol{\lambda}_d + \boldsymbol{K}_\lambda \boldsymbol{\Delta \lambda} - \boldsymbol{\nabla}_q \boldsymbol{\lambda} \dot{\boldsymbol{q}}_{id} \right) \end{aligned} \tag{18}$$

Our trajectory generator does not take the compliant foot-ground contact into account, i. e. foot trajectories are planed to not penetrate the environment. This means that for $\boldsymbol{q} = \boldsymbol{q}_{id}$, the contact element deformations $\boldsymbol{d}_{c,i}$ and the corresponding contact force $\boldsymbol{\lambda}$ vanish and $\boldsymbol{\nabla}_q \boldsymbol{\lambda} \dot{\boldsymbol{q}}_{id} \equiv 0$. Using this relationship we obtain the following reference trajectory modification:

$$\boldsymbol{\Delta \dot{x}}_\lambda = \left(\boldsymbol{S}_\lambda \boldsymbol{\nabla}_q \boldsymbol{\lambda} \left(\bar{\boldsymbol{S}}_x \boldsymbol{\nabla}_q \boldsymbol{x} \right)^\dagger \right)^\dagger \boldsymbol{S}_\lambda \left(\boldsymbol{\dot{\lambda}}_d + \boldsymbol{K}_\lambda \boldsymbol{\Delta \lambda} \right) \tag{19}$$

For the ideal case of an exact contact model and no disturbances, the term due to $\boldsymbol{\dot{\lambda}}_d$ leads to $\boldsymbol{\lambda} = \boldsymbol{\lambda}_d$, i. e. the reference trajectory modification compensates the deformations in the foot-ground contact. Alternatively, we could take the compliant contact into account in the trajectory planner. In this case the terms $\boldsymbol{\nabla}_q \boldsymbol{\lambda} \dot{\boldsymbol{q}}_{id}$ and $\boldsymbol{\dot{\lambda}}_d$ in (18) would cancel, leading to the same trajectory modification.

Due to the varying contact state, we cannot use (19) directly. For the swing leg all contacts are inactive, $\boldsymbol{\nabla}_q \boldsymbol{\lambda}$ becomes singular and we cannot compute the pseudoinverse in (19). Since the contact force is independent of the trajectory modification $\boldsymbol{\Delta \dot{x}}_\lambda$, we blend from force to position control for DoFs with vanishing contact stiffness:

$$\begin{aligned} \boldsymbol{\Delta \dot{x}}_\lambda = &\Big\{ \left[\boldsymbol{S}_\lambda \boldsymbol{\nabla}_q \boldsymbol{\lambda} (\bar{\boldsymbol{S}}_x \boldsymbol{\nabla}_q \boldsymbol{x})^\dagger \right]^\dagger \boldsymbol{\alpha}_\lambda \boldsymbol{S}_\lambda \big[\boldsymbol{K}_{\lambda,\mathrm{ff}} \boldsymbol{\dot{\lambda}}_d + \\ &\boldsymbol{K}_\lambda (\boldsymbol{\lambda}_d - \boldsymbol{\lambda}) \big] \Big\} + \boldsymbol{\alpha}_x \big[\bar{\boldsymbol{S}}_x \boldsymbol{K}_{\lambda x} (\boldsymbol{x}_d - \boldsymbol{x}) \big] \end{aligned} \tag{20}$$

Here $\boldsymbol{\alpha}_\lambda + \boldsymbol{\alpha}_x = \boldsymbol{E}, \alpha_{i,jk} \in [0,1]$ are gain matrices determining which DoFs are position or force controlled. Additionally, a damping term is added to each vanishing row of $\boldsymbol{\nabla}_q \boldsymbol{\lambda}$, to enable calculation of the pseudoinverse. Since the corresponding elements in $\boldsymbol{\alpha}_\lambda$ are zero, the magnitude of the damping term does not influence the result of (20).

The actual contact dynamics are more complex than the model (11) used in the controller. We therefore introduce the additional control gain $\boldsymbol{K}_{\lambda,\mathrm{ff}}$ to modify the feed-forward term in (20). This parameter is tuned manually during walking experiments.

After adding the modification (20) to the original reference trajectory, we must map the modified reference $\boldsymbol{x}_d$ to the generalized coordinates $\boldsymbol{q}$. If we choose $\dim(\boldsymbol{x}) < \dim(\boldsymbol{q})$, as we have done for *LOLA*, this mapping is not unique. For calculating the desired generalized coordinates $\boldsymbol{q}_d$, we chose the resolved motion rate control method originally proposed by WHITNEY [23] combined with the minimization of an objective function H in the null-space of $\boldsymbol{\nabla}_q \boldsymbol{x}$, as proposed

by LIÉGEOIS [24]:

$$\begin{aligned}\dot{\boldsymbol{x}}_d &= \dot{\boldsymbol{x}}_{id} + \bar{\boldsymbol{S}}_x^T \boldsymbol{\Delta}\dot{\boldsymbol{x}}_\lambda + \frac{\boldsymbol{K}_x}{\Delta t}\left(\boldsymbol{\Delta}\boldsymbol{x}_{\text{pos}} + \bar{\boldsymbol{S}}_x^T \boldsymbol{\Delta}\boldsymbol{x}_\lambda\right)\\ \boldsymbol{\Delta}\boldsymbol{x}_\lambda &= \int \boldsymbol{\Delta}\dot{\boldsymbol{x}}_\lambda dt\\ \dot{\boldsymbol{q}}_d &= (\boldsymbol{\nabla}_q \boldsymbol{x})^\dagger \dot{\boldsymbol{x}}_d - \alpha_N \boldsymbol{N}\boldsymbol{\nabla}_q H\\ \boldsymbol{q}_d &= \int \dot{\boldsymbol{q}}_d dt\end{aligned} \tag{21}$$

Here $\boldsymbol{N}$ is the null-space projection matrix, α_N a gain for minimizing the objective function H, Δt is the time step and $\boldsymbol{\Delta}\boldsymbol{x}_{\text{pos}} = \boldsymbol{x}_{id} - \boldsymbol{x}$.

Without null-space optimization, (21) gives the least squares solution for $\dot{\boldsymbol{q}}_d$, leading to a local minimization of joint velocities.

We currently use the objective function H to avoid joint limits and to choose symmetric and "comfortable" poses. For both components we use quadratic cost functions. However, joint limit avoidance is only activated close to the edges of the working range (cf. Fig. 5).

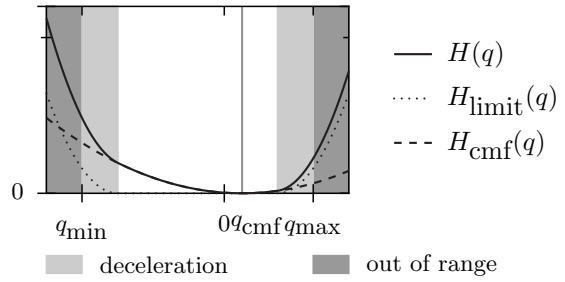

Fig. 5. Schematic representation of the objective function H for a single joint. $H_{\text{limit}}, H_{\text{cmf}}$ are the terms for joint limit avoidance and convergence towards the preferred joint angle q_{cmf} respectively.

C. Run-Time Performance

To reduce the computational cost during real-time control, we avoid explicitly calculating pseudo-inverses and null-space projection matrices. Instead, we solve two linear systems of equations as proposed by KLEIN and HUANG [25]. On the on-board computers (Intel T7600 mobile CPU, 2.33 GHz, 32-bit mode) the average run-time for a single threaded version of the proposed stabilizing control is 393 μs for *JOHNNIE* and 720 μs for *LOLA*. While this is fast enough for an overall control cycle of 1.5 ms, the results also show that the run-time strongly increases with the number of DoFs. However, on a more recent desktop CPU (Intel E8400, 3.0 GHz, 64-bit mode) the execution time for *LOLA* is reduced to 211 μs. The authors also believe that there still is much room for optimization in the current code, so it should be possible to further reduce the run-time, making the proposed approach applicable to systems with more DoFs.

V. RESULTS AND DISCUSSION

The proposed control system has been analyzed in simulations of *JOHNNIE* and *LOLA* and walking experiments with *JOHNNIE*.

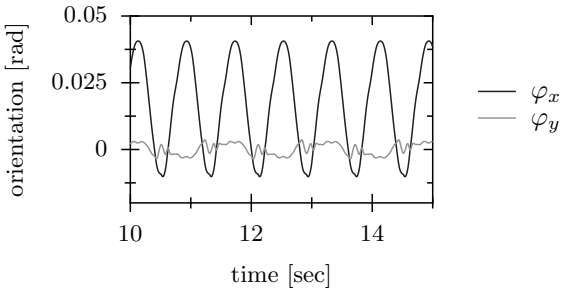

Fig. 6. Simulation of *LOLA*'s upper body oscillations while walking in a straight line. φ_x, φ_y are the angles between the upper body and the gravity vector in the sagittal and lateral plane respectively.

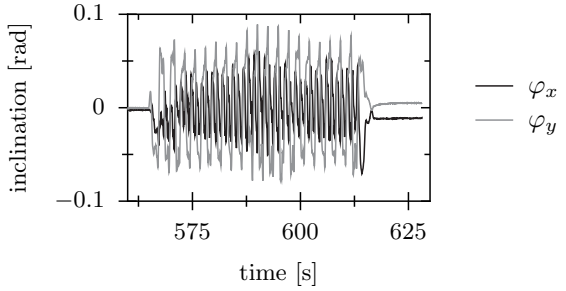

Fig. 7. Measurement of *JOHNNIE*'s upper body oscillations while walking in a circle. φ_x, φ_y are the angles between the upper body and the gravity vector in the sagittal and lateral plane respectively.

Fig. 6 shows the upper body oscillations for *LOLA* walking in a straight line calculated using a refined version of the simulation program described in [26] and Fig. 1 a snapshot of an animation including the planned walking pattern.

Figs. 8 and 7 show snapshots of walking experiments with *JOHNNIE* and *JOHNNIE*'s upper body orientation measured with the on-board IMU respectively. The upper body oscillations are not perfectly periodic, since the desired average walking speed and direction was controlled by a joystick and therefore constantly changing.

The results show that reliable walking in arbitrary directions and with arbitrary curvature is possible and disturbances are rejected effectively.

Furthermore, the control system is quite flexible and many extensions and modifications are easily implemented. For example, adding an integral action to the force control to improve disturbance rejection is achieved by simply adding $\boldsymbol{K}_{\lambda,\text{INT}} \int \boldsymbol{\Delta}\boldsymbol{\lambda} dt$ in (14). Another straight-forward addition to the control framework is the on-line adaptation of model parameters, especially of the ground contact stiffness.

Future work will include refining the proposed control system by incorporating more precise models in order to further improve performance and evaluating the method in walking experiments with *LOLA*.

REFERENCES

[1] I. S. Department. (2008) World robotics 2008. [Online]. Available: http://www.worldrobotics.org/

[2] M. Hirose and K. Ogawa, "Honda humanoid robots development," *Phil. Trans. R. Soc. A*, vol. 365, pp. 11–19, 2006.

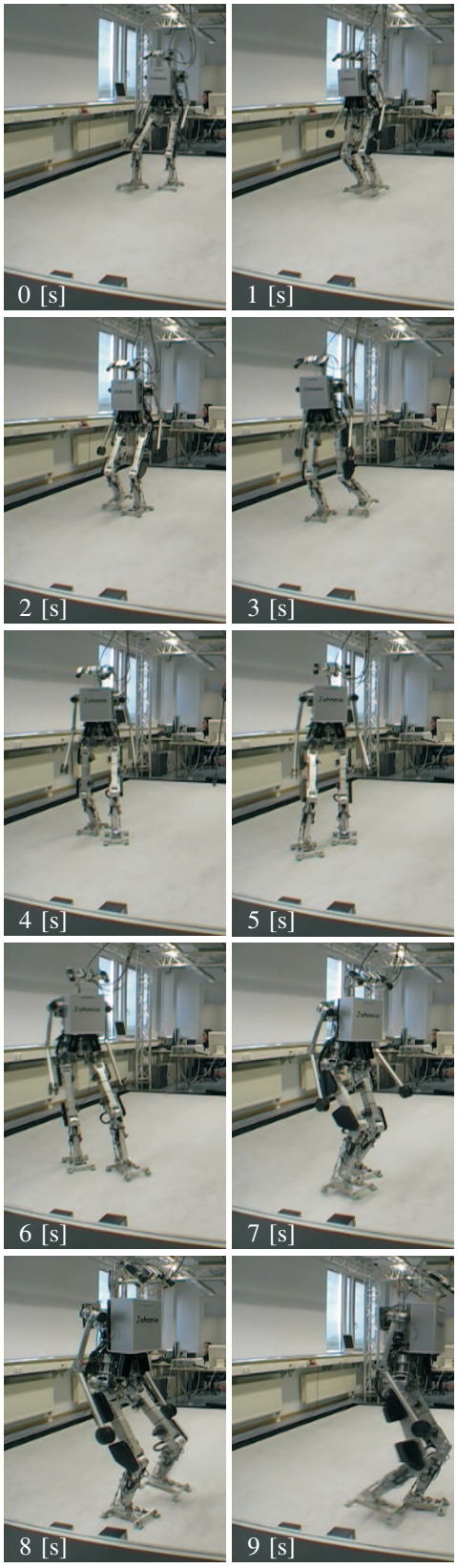

Fig. 8. Snapshots of *JOHNNIE* walking with the proposed control system.

[3] T. Tajima, D. Honda, and K. Suga, "A fast running experiment involving a humanoid robot," in *RSJ2008*, 2008.

[4] K. Kaneko, F. Kanehiro, S. Kajita, H. Hirukawa, T. Kawasaki, M. Hirata, K. Akachi, and T. Isozumi, "Humanoid robot HRP-2," in *Proc of the 2004 IEEE Intl Conf on Robotics and Automation*, New Orleans, USA, apr 2004.

[5] K. Nishiwaki, J. Kuffner, S. Kagami, M. Inaba, and H. Inoue, "The experimental humanoid robot H7: a research platform for autonomous behaviour," *Phil. Trans. R. Soc. A*, vol. 365, no. 1850, pp. 79–107, 2006.

[6] K. Löffler, M. Gienger, F. Pfeiffer, and H. Ulbrich, "Sensors and control concept of a biped robot," *IEEE Trans. Ind. Electron.*, vol. 51, no. 5, pp. 972–980, 2004.

[7] S. Lohmeier, T. Buschmann, and H. Ulbrich, "Humanoid robot lola," in *Proc IEEE Int Conf Robotics and Automation (ICRA)*, 2009.

[8] T. Buschmann, S. Lohmeier, M. Bachmayer, H. Ulbrich, and F. Pfeiffer, "A collocation method for real-time walking pattern generation," in *Proc IEEE-RAS Int Conference on Humanoid Robotics (Humanoids)*, 2007.

[9] S. Kajita, F. Kanehiro, K. Kaneko, K. Fujiwara, K. Harada, K. Yokoi, and H. Hirukawa, "Biped walking pattern generation by using preview control of zero-moment point," in *Proc of the IEEE Intl Conf on Robotics & Automation*, Taipei, Taiwan, sep 2003.

[10] T. Buschmann, S. Lohmeier, H. Ulbrich, and F. Pfeiffer, "Optimization based gait pattern generation for a biped robot," in *Proc IEEE-RAS Int Conference on Humanoid Robotics (Humanoids)*, Tsukuba, Japan, dec 2005.

[11] S. Kajita, T. Nagasaki, K. Kaneko, K. Yokoi, and K. Tanie, "A running controller of humanoid biped HRP-2LR," in *Proc IEEE Int Conf Robotics and Automation (ICRA)*, 2005.

[12] T. Takenaka, "Controller of legged mobile robot," European Patent Application, 11 2004.

[13] K. Nishiwaki and S. Kagami, "High frequency walking pattern generation based on preview control of zmp," in *Proc IEEE Int Conf Robotics and Automation (ICRA)*, 2006.

[14] F. Pfeiffer and R. Johanni, "A concept for manipulator trajectory planning," in *Proc IEEE Int Conf Robotics and Automation (ICRA)*, 1986.

[15] C. Chevallereau, D. Djoudi, and J. Grizzle, "Stable bipedal walking with foot rotation through direct regulation of the zero moment point," *IEEE Trans. Robot. Automat.*, vol. 24, pp. 390–401, 2008.

[16] K. Nishiwaki, "Design of walking system and online control of a humanoid robot." Ph.D. dissertation, University of Tokyo, 2001.

[17] Y. Fujimoto and A. Kawamura, "Proposal of biped robust hybrid walking control based on position/force control," in *Proc IEEE Int Conf Robotics and Automation (ICRA)*, 1996.

[18] S. Kajita and K. Tani, "Experimental study of biped dynamic walking in the linear inverted pendulum mode," in *Proc IEEE Int Conf Robotics and Automation (ICRA)*, Leuven, Belgium, 1995, pp. 2885–2891.

[19] J. Craig and M. Raibert, "A systematic method of hybrid position/force control of a manipulator," in *Computer Software and Applications Conference, IEEE Computer Society*, 1979.

[20] O. Khatib, "A unified approach for motion and force control of robot manipulators: The operational space formulation," *IEEE Trans. Robot. Automat.*, vol. 1, pp. 43–53, 1987.

[21] A. Albu-Schäffer and G. Hirzinger, "Cartesian impedance control techniques for torque controlled light-weight robots," in *Proc IEEE Int Conf Robotics and Automation (ICRA)*, 2002.

[22] B. Siciliano and O. Khatib, Eds., *Springer Handbook of Robotics*. Springer-Verlag Berlin Heidelberg, 2008.

[23] D. E. Whitney, "Resolved Motion Rate Control of Manipulators and Human Prostheses," *IEEE Transactions on Man Machine Systems*, vol. 10, no. 2, pp. 47–53, June 1969.

[24] A. Liégeois, "Automatic supervisory control of the configuration and behavior of multibody mechanisms," *IEEE Intl. Transactions on Systems, Man, and Cybernetics*, vol. SMC-7, no. 12, pp. 63–71, 1977.

[25] Y. Nakamura, *Advanced Robotics: Redundancy and Optimization*. Addison-Wesley, 1991.

[26] T. Buschmann, S. Lohmeier, H. Ulbrich, and F. Pfeiffer, "Modeling and simulation of a biped robot," in *Proc of the 2006 IEEE Intl Conf of Intelligent Robots and Systems*, 0rlando, USA, may 2006.